

# Structural Changes to the Calcium–Silicate–Hydrate Gel Phase of Hydrated Cement with Age, Drying, and Resaturation

Jeffrey J. Thomas,<sup>†,‡</sup> Andrew J. Allen,<sup>§</sup> and Hamlin M. Jennings<sup>†,¶</sup>

<sup>‡</sup>Department of Civil and Environmental Engineering, Northwestern University, Evanston, Illinois 60208

<sup>§</sup>Materials Science and Engineering Laboratory, National Institute of Standards and Technology, Gaithersburg, Maryland 20899

<sup>¶</sup>Department of Materials Science and Engineering, Northwestern University, Evanston, Illinois 60208

The effects of drying to various relative humidity (RH) levels on the internal structure of hydrated cement paste were investigated using small-angle neutron scattering (SANS). Specimens of young and mature portland cement paste were analyzed in the initial saturated state, in the dried state, and then again after resaturation, allowing reversible and irreversible effects to be separated. While the observed changes on drying are mainly physical in nature, the ability of the microstructure to resist permanent structural rearrangement increased over time as the hydration and aging reactions progressed. Permanent changes to the nanometer-to-micrometer scale microstructure induced by drying were quantified by applying a fractal model to the SANS data for resaturated pastes. At RH levels above  $\approx 54\%$ , capillary stresses compact the nanometer-level pore structure of the calcium–silicate–hydrate (C–S–H) gel phase, increasing the gel density by a mechanism related to that governing the classical “constant rate period” for pure gels. Owing to the restraining effects of the other solid phases in cement paste, this decrease in the volume of the C–S–H gel also increases the intensity of surface fractal scattering that arises from the deposition of hydration product onto the surface of the reacting cement particles. At all RH levels, but particularly below 54%, drying decreases the measured total internal surface area of the specimens. This is attributed to a loss of surface area at particle contacts as the average separation distance between adjacent C–S–H gel nanoparticles decreases on drying.

## I. Introduction

HARDENED cement paste, the binder component of concrete, forms by a series of parallel chemical reactions between cement powder and water, resulting in a complex microstructure containing significant amounts of liquid, chemically bound and physically bound water. As the hydration reactions proceed, the water-filled space in cement paste is increasingly replaced with solid hydration product, increasing its strength and decreasing its permeability. Of the several hydrated phases, the most abundant and important is the calcium–silicate–hydrate (C–S–H) gel, a precipitated colloid with a structure generically similar to that of inorganic silicate gels.<sup>1</sup> Owing to its nanoscale pore system and high water content, the C–S–H gel is the primary phase affected by drying of cement paste. Although the nanoscale

structure of the amorphous C–S–H gel is not completely understood, small-angle neutron scattering (SANS) and other evidence indicate that it exhibits underlying (universal) fractal-scaling characteristics that can be analyzed through application of a fractal microstructure model. Previous SANS studies indicate a structure composed of particles with a characteristic size of about 5 nm that are aggregated into a relatively dense volume fractal structure.<sup>2–5</sup> The properties of cement paste also undergo changes with time that are not directly associated with the hydration reactions referred to as aging. These changes are often attributed to an increase in the average degree of polymerization of the silicate structure of C–S–H gel after it forms.<sup>6</sup>

Drying of cement paste, which occurs naturally on exposure to low-humidity environments, causes a number of undesirable effects that limit concrete performance and durability, including macroscopic volume changes (drying shrinkage), cracking, and an increase in permeability. In addition, drying stops the hydration reactions, and these reactions may not fully restart when the cement is rewetted. The ability of concrete to resist damage on drying improves with its age, and drying of young concrete can significantly limit its durability and thus its service life. Recent efforts have been made to model and predict drying shrinkage by modeling the underlying physical phenomena taking place at different length scales within the microstructure.<sup>7–9</sup> These efforts are somewhat limited at present by a lack of quantitative information about the physical and chemical changes induced by drying, particularly to the nanometer-level structure of the C–S–H gel.

The response of cement paste and concrete to drying is most commonly and easily analyzed by measuring the reversible and irreversible components of the bulk linear shrinkage strain, both of which increase continuously as the relative humidity (RH) inside the paste decreases. Well-defined regimes have been identified,<sup>10</sup> indicating that different shrinkage mechanisms are operational at different RH levels. However, the shrinkage process of cement paste is complicated by the presence of unshrinking solid phases such as calcium hydroxide crystals and the cores of unhydrated cement particles that restrain the shrinkage of the C–S–H gel phase. As a result, relatively small bulk dimensional changes may be associated with large deformations of certain parts of the microstructure and large internal stresses.<sup>11</sup> Under these conditions, obtaining a full understanding of the effects of drying requires probing the microstructure directly.

In the present study, the effects of drying on the internal structure of cement paste are investigated using SANS. Because the scattering from different sized features occurs at different scattering angles, SANS can separate structural changes occurring at different length scales within the microstructure. SANS is particularly useful for investigating cement paste because it is sensitive to features over the scale range from 1 to 100 nm that

P. Brown—contributing editor

Manuscript No. 24128. Received December 19, 2007; approved July 8, 2008.

The work performed at Northwestern University was supported by the National Science Foundation under contract CMS 0409571. The work at NIST utilized facilities supported in part by the National Science Foundation under Agreement No. DMR-9986442.

<sup>†</sup>Author to whom correspondence should be addressed. e-mail: jthomas@northwestern.edu

dominate the microstructure, and it can be performed on both saturated and dry specimens. Thin cement paste specimens of two different ages were measured first in their natural saturated state, then after drying to various RH levels, and then again after subsequent resaturation, allowing both reversible and irreversible microstructural changes to be determined. Through application of a practical fractal microstructure model, the present results give a more complete picture of the structural changes associated with the drying of cement paste than has previously been available.

## II. Experimental Procedure

### (1) Sample Preparation and Analysis

All experiments were performed using a commercial white portland cement (WPC) (US Gypsum Corp., Chicago, IL<sup>12</sup>). The mineral composition by mass of the WPC is 72% tricalcium silicate, 17% dicalcium silicate, 5% tricalcium aluminate, 1% tetracalcium ferrite, and 0.7% alkalis (Na<sub>2</sub>O and K<sub>2</sub>O). Fresh pastes were mixed at a water-to-cement ratio of 0.5 by mass and cast into cylindrical polystyrene vials measuring 25 mm diameter by 50 mm high. After 3 days, the hardened pastes were demolded and further hydrated in a saturated Ca(OH)<sub>2</sub> solution for a total of either 8 days (referred to as young paste) or 3 years (mature paste). The pastes were cut into 0.6-mm thick coupons using a water-lubricated wafering saw before the drying treatment. For the young pastes, the age of 8 days represents the age at the start of drying, as cement hydration ceases as soon as the drying treatment causes the internal RH to fall below about 90%.

Coupons of young WPC paste were dried to RH levels of 76%, 54%, 33%, and 0%, while mature pastes were dried to 54% and 0% only. The effects of drying are thus determined from parallel specimens cut from the same block of paste. To dry to RH levels above 0%, coupons were placed in a sealed desiccator containing a saturated salt solution with the appropriate equilibrium vapor pressure of water, which was verified with a humidity monitor. Drying to 0% RH was accomplished by evacuating a desiccator with a rotary vacuum pump. Specimens were exposed only to pure nitrogen during the drying process so as to avoid reaction with carbon dioxide in the air, which occurs rapidly in partially dried cement paste. Most of the weight loss on drying the thin coupons occurs in the first 48 h, but a slow rate of weight loss continues for several days thereafter. All specimens were dried for 7 days. It should be noted that specimens equilibrated to the lower humidity levels (0% and 33% RH) are subjected only briefly to the capillary stresses associated with the higher humidity levels, and thus the microstructural effects of drying are not necessarily expected to increase monotonically with decreasing RH.

Resaturation was accomplished by placing dried coupons into a saturated Ca(OH)<sub>2</sub> solution for a 24-h period leading up to the SANS measurement. In contrast to the drying process, the resaturated weight stabilized within hours. The weight of fully resaturated coupons closely matched the original saturated weight, which is evidence of a lack of carbonation (which causes a weight gain). All specimens were sealed into small specimen holders just before the SANS measurement to avoid any change in sample condition during the measurement. Undried control specimens of the correct age were also measured in a fully saturated state.

The SANS measurements were performed during a 24-h period using the 30-m NG7 SANS instrument<sup>13</sup> at the NIST Center for Neutron Research, National Institute of Standards and Technology, Gaithersburg, MD, using a neutron wavelength of  $\lambda = 0.8$  nm. The scattered neutron intensity was recorded on a two-dimensional position sensitive detector. These data were summed radially to obtain the SANS intensity,  $I(q)$ , as a function of the magnitude of the scattering vector, defined as  $q = (4\pi/\lambda)\sin(\theta/2)$ , where  $\theta$  is the scattering angle. Three SANS sample-to-detector configurations were used, giving an effective

$q$ -range of 0.02–2.2 nm<sup>-1</sup>. The volume of the specimen penetrated by the beam was approximately 16 mm<sup>3</sup>, large enough to be representative of the bulk cement paste and many orders of magnitude larger than the features causing the scattering. Thus, all micro- and nanostructural parameters derived from the SANS data are statistically representative of the specimen as a whole.

### (2) Interpretation of the SANS Data

As anhydrous cement powder reacts with water, hydration products build up in an increasingly thick layer around the shrinking cores of the dissolving particles, creating a complex microstructure that is heterogeneous over extended length scales. A model for fitting the scattering response over almost the entire accessible  $q$ -range has previously been developed by Allen and colleagues<sup>2–4</sup> and used to analyze the changes that occur during the progress of hydration and with the addition of additives such as blast furnace slag and silica fume. This model is based on spheroidal C–S–H particles with fixed aspect ratios that can be varied from 0.5 (oblate) to 2 (prolate). The characteristic size of the particles, obtained from the fits, is always close to 5 nm for cement paste. The size and particularly the shape of the C–S–H particles is a matter of active research and discussion, and may depend on local conditions at the time of formation, such as available space and solution composition. AFM studies<sup>14</sup> have reported that the primary C–S–H gel particles have a lamellar, or sheet-like shape, with a thickness of 5 nm but up to 60 nm in width, while TEM studies,<sup>15</sup> on the other hand, have presented evidence for elongated or fibrous particles, also with a minimum dimension of a few nanometers. Jennings<sup>16</sup> has recently proposed, based primarily on water sorption experiments, that the fundamental C–S–H particles are brick shaped, a hypothesis that is generally compatible with the SANS interpretation. It should be noted that the SANS response from cement paste does not exhibit any of the hallmarks of a fibrous or sheet-like morphology at length scales greater than several nanometers, unless the C–S–H phase is decalcified.<sup>17</sup>

Application of the model to the scattering data relies on the observed scale separation between three scattering regimes associated with surface fractal, volume fractal, and single-particle scattering (see Fig. 1), so that scattering in each regime is fitted with only around three parameters. At lower  $q$  values (corresponding to larger microstructural features), the deposition of hydration product onto the cement particles creates a rough surface that generates surface fractal scattering. At intermediate  $q$  values, scattering is dominated by a volume fractal structure with a scaling exponent between 2.5 and 2.7 created by the random agglomeration of the fundamental C–S–H particles. At high  $q$  values, single-particle scattering applies and the form factor for single-particle scattering from a spheroid,  $F^2(q)$ , is used.<sup>18</sup> The spheroids have radius  $\beta R_0$  along one axis, where  $\beta$  is close to 1. The full-model equation is

$$I(q) = \phi_{\text{CSH}} V_p \Delta \rho^2 \left\{ \frac{\eta R_c^3}{\beta R_0^3} \left( \frac{\xi_v}{R_c} \right)^{D_v} \times \frac{\sin[(D_v - 1) \arctan(q \xi_v)]}{(D_v - 1) q \xi_v [1 + (q \xi_v)^2]^{(D_v - 1)/2}} + (1 - \eta)^2 \right\} F^2(q) + \frac{\pi \xi_s^4 \Delta \rho^2 S_0 \Gamma(5 - D_s) \sin[(3 - D_s) \arctan(q \xi_s)]}{[1 + (q \xi_s)^2]^{(5 - D_s)/2} q \xi_s} + \text{BGD} \quad (1)$$

where  $\phi_{\text{CSH}}$  is the volume fraction of solid C–S–H gel particles,  $V_p$  is the volume of a single C–S–H particle ( $= 4\pi\beta R_0^3/3$ ),  $R_c$  is the sphere-equivalent mean diameter (calculated from  $R_0$  and  $\beta$ ), and  $\eta$  is the local packing fraction for nearest neighbor particles

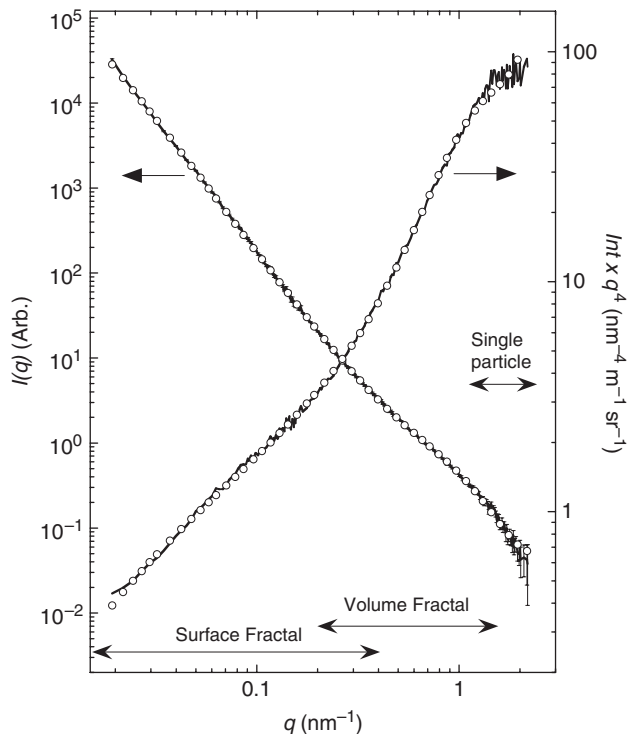


**Fig. 1.** Small-angle neutron scattering data for white portland cement paste hydrated for 8 days and never dried, plotted in two different ways. The lines are the data and the open circles are model fits using Eq. (1). Error bars are shown on the  $I(q)$  versus  $q$  plot. Approximate  $q$ -ranges for each scattering regime fit using Eq. (1) are shown.

that represents the local density from which the volume fractal scales.  $D_V$  and  $D_S$  are the volume and surface fractal scaling exponents, and  $\xi_V$  and  $\xi_S$  are the upper-limit length scales (correlation lengths) over which volume and surface fractal scaling apply.  $S_0$  is the smooth geometric surface area on which

the surface fractal microstructure is deposited, i.e., it ignores all roughness at length scales smaller than  $\xi_S$ . The neutron scattering contrast,  $|\Delta\rho^2|$ , is discussed below. The background term, BGD, allows the data to be uniformly adjusted to account for incoherent scattering from the sample. In practice, fitted values of  $R_0$  for  $\beta > 1$  and  $\beta < 1$  (prolate and oblate spheroids) are each converted to a sphere-equivalent radius, and then these values are averaged and doubled to give the diameter of the C-S-H building-block particles,  $a_S$ , reported here.

The first term in Eq. (1), which gives the volume-fractal<sup>19</sup> and single-particle scattering, has also been used to model the scattering from fine silica gels prepared using sol-gel methods.<sup>20–23</sup> The second term in Eq. (1) is the surface fractal scattering.<sup>24</sup> It is important to note that Eq. (1) cannot be fitted with all parameters varying freely and simultaneously. The fits do not generally converge to a stable result if  $\eta$ , BGD and  $R_0$  are allowed to vary simultaneously. For spheres the gel particle diameter  $a_S$  is the same as  $R_C$  and this can be determined from the high- $q$  cut-off in the volume-fractal scattering. The local-packing fraction,  $\eta$ , can then be determined and compared in a series of similar fits (as here) from the relative prominence of the volume-fractal and form-factor scattering components.

During the first few days of hydration, as hydration product with an internal nanoscale pore system fills in the larger capillary pore space between hydrating cement grains, the volume fractal intensity increases. Meanwhile, the scattering at lower  $q$  decreases as coarse cement particles are consumed in the hydration reactions and the sharp interface between the cement particles and the larger pores is softened by the deposition of fractal hydration product. Hydration then continues at a slower rate, generating a denser form of hydration product within the boundaries of the original cement particles that contributes little to the SANS intensity.<sup>25</sup> However, the volume fractal morphology continues to grow at a relatively slow rate for some weeks.

Figure 1 shows the SANS data for the undried young paste along with the fit to the model of Eq. (1). Both  $I(q)$  and  $I(q)q^4$  are plotted on log-log plots versus  $q$ ; the latter form accentuates differences between related datasets and is used in Figs. 2 and 3

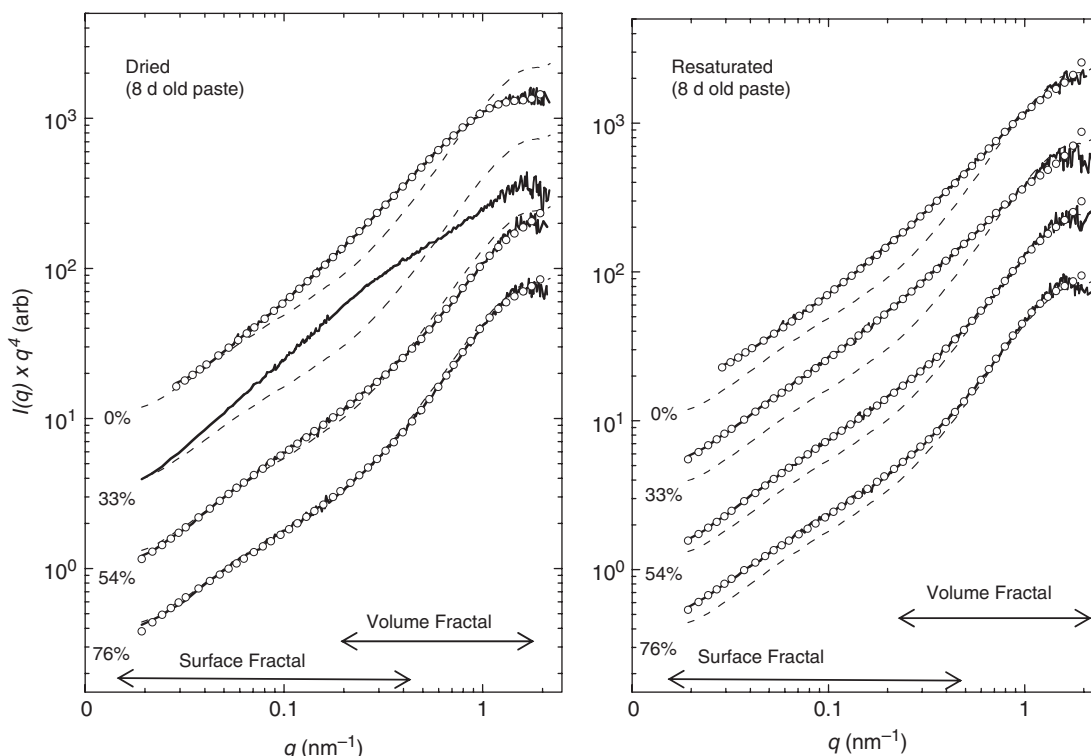


**Fig. 2.** Small-angle neutron scattering data (solid lines) from young cement paste specimens after drying to various relative humidity (RH) levels (left) and after subsequent resaturation (right). Data for different RH levels are offset. The open circles are fits using the fractal model given by Eq. (1). The dotted lines are the data from the undried control (also shown in Fig. 1), which are repeated at each offset.

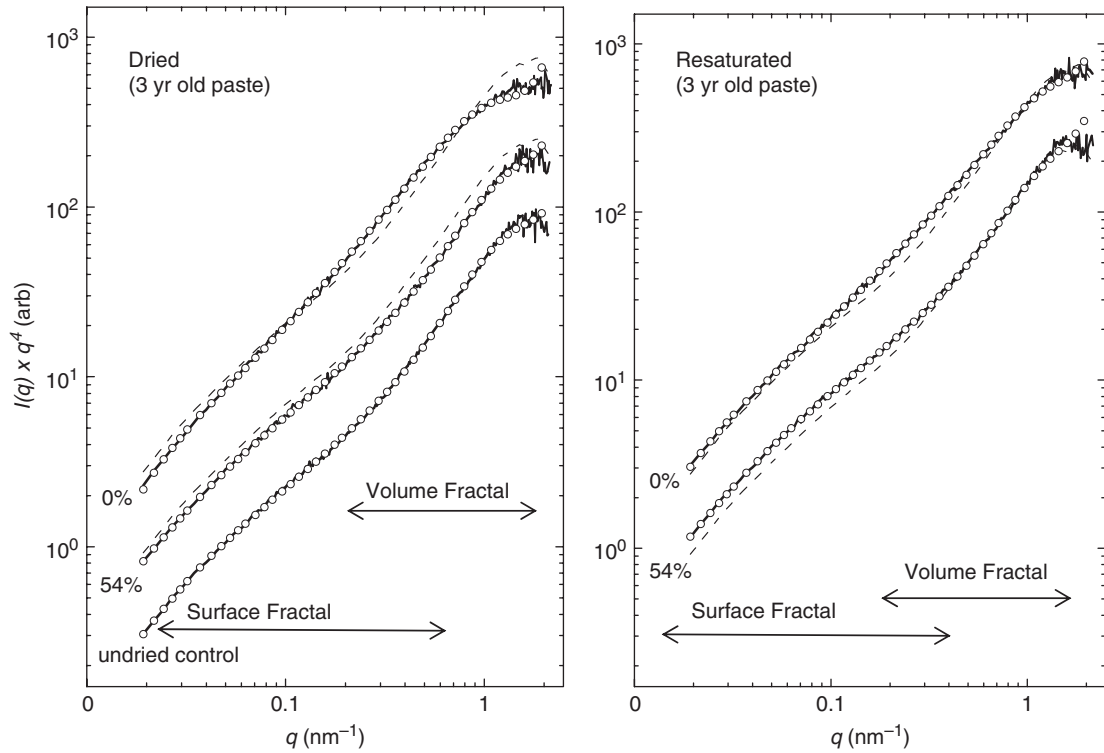


**Fig. 3.** Small-angle neutron scattering data (solid lines) from mature cement paste specimens after drying to 50% and 0% relative humidity (RH) (left), and after subsequent resaturation (right). Data for different RH levels are offset. The open circles are fits using the fractal model given by Eq. (1). The dotted lines are the data from the undried control (also shown with fit at left), which are repeated at each offset.

to present the drying results. The fit is quite good over two decades of  $q$  and six decades of intensity, supporting the general physical interpretation on which the model is based. The model deviates somewhat from the data at the highest  $q$  values where the fractional uncertainties are high after the flat background subtraction, and the Bessel function oscillations for an ideal spheroid, incorporated in  $F^2(q)$ , are not observed for a real, nonideal, particle shape. In fact, when  $qD_{\min} \gg 1$ , where  $D_{\min}$  is the size of the smallest features,  $I(q) \sim q^{-4}$  according to Porod's law. Porod's law can be applied to the coherent (i.e. background subtracted) data in this scattering regime to calculate the total internal surface area of the specimen per unit specimen volume,  $S_T$ :

$$S_T = \frac{C_P}{2\pi|\Delta\rho|^2} \quad (2)$$

where  $C_P$  is the constant of proportionality for the Porod scattering and  $|\Delta\rho|$  is the difference in the neutron scattering length density of the two phases causing the scattering. For cementitious systems, the Porod scattering can be recovered from the coherent-scattering data above  $q \cong 1.4 \text{ nm}^{-1}$ . Above about  $q = 2 \text{ nm}^{-1}$  the Porod scattering can no longer be statistically separated from the incoherent flat background scattering.<sup>25</sup> The surface area of cement paste arises mainly from the C-S-H gel, with only small contributions from other phases such as calcium hydroxide, and is about two orders of magnitude larger than that of the starting cement powder. Note that while the C-S-H nanoparticles likely have an internal layered structure into which water can leave and enter, these layers are too small to cause scattering in the accessible  $q$  range.

The neutron-scattering contrast,  $|\Delta\rho|^2$ , describes the intrinsic strength of the neutron-scattering interaction at the interface between two scattering phases, and can be thought of as a structure-independent-scaling factor for the SANS intensity. An independent determination of the contrast is necessary to obtain values of  $\phi_{\text{CSH}}$  from Eq. (1) and values of  $S_T$  from Eq. (2). In a multiphase system, the contrast will vary with  $q$  depending on the relative prominence of each phase at the

associated length scale. For cementitious materials under normal conditions, the interface between solid C-S-H gel and the water-filled pore system dominates at all  $q$ -values accessed, with a small contribution from calcium hydroxide. The neutron scattering contrast in saturated cement paste was recently determined accurately from SANS measurements involving deuterated fluid exchange and from SANS/SAXS intensity comparisons to be  $|\Delta\rho|^2 = 9.64 \times 10^{28} \text{ m}^{-4}$ .<sup>26</sup> In a fully dried specimen, the pore system contains air rather than water, causing the associated value of  $\rho$  to increase from  $-0.56 \times 10^{14} \text{ m}^{-2}$  to 0. In addition, some of the structural water associated with the solid C-S-H gel is removed on drying, causing the value of  $\rho$  for the solid phases to increase from  $2.54 \times 10^{14} \text{ m}^{-2}$  to approximately  $2.81 \times 10^{14} \text{ m}^{-2}$ . The net result is that the scattering contrast decreases to around  $7.9 \times 10^{28} \text{ m}^{-4}$ , corresponding to a nearly 20% decrease in  $I(q)$ .

Interpretation of the SANS response from partially dried specimens is more complicated. At higher RH levels (e.g., 76%), the system has effectively three phases (solid, liquid, and air) and additional scattering can arise from the interface between the liquid phase and the emptied pores.<sup>27</sup> At lower RH levels (e.g., 33% RH), the liquid water in cement paste is present primarily as an adsorbed layer around the individual gel particles with a thickness comparable to the neutron wavelength. Such a layer would reduce the observed specific surface area by filling in the small spaces between gel particles,<sup>28</sup> and could also change the effective scattering contrast between the solid phase and emptied pores in a way that is difficult to quantify. These issues do not apply to pastes that have been resaturated after drying; any observed changes in the SANS response in this case can be unambiguously attributed to structural changes to the solid phase induced by drying. The quantitative analysis presented here therefore focuses on the saturated and resaturated specimens.

### III. Results and Discussion

Figure 2 shows SANS data for young WPC pastes after drying to various RH levels and after subsequent resaturation, along

with fits to Eq. (1) (plotted as open circles). Satisfactory fits using Eq. (1) could be obtained for all of the resaturated datasets and for most of the dried datasets, using values of the microstructural parameters that are not significantly different from those obtained for the undried controls (see Fig. 4). Thus, a key finding of the present study is that drying of cement paste does not radically alter the fine structure. However, statistically significant shifts in the SANS data, corresponding to significant microstructural changes, were observed (note that the two-

decade change in intensity with  $q$  tends to compress the differences between datasets in Figs. 2 and 3). On drying to the higher humidity levels (76% RH and to 54% RH), the shape of the dried datasets underwent subtle changes from the control (shown as dotted lines at each offset). After resaturation, it can be seen that the scattering associated with the surface fractal component is irreversibly increased by high-RH drying while that associated with the volume fractal component is nearly unchanged. The increase in surface fractal intensity on resaturation can be attributed to the greater scattering contrast when the larger pores contain water rather than air, and thus is not a microstructural effect.

Drying to lower RH levels (33% and 0% RH) caused additional changes to the SANS data. In the dry state, the volume fractal and Porod intensities are significantly reduced. On resaturation these intensities recover somewhat, but there remains an irreversible change in the apparent volume fractal slope that makes the two fractal regions less distinct. The surface fractal scattering is irreversibly increased as was also observed on drying to higher humidity levels. The data from the 33% RH-dried paste exhibits a “hump” at intermediate  $q$  values that disappears on resaturation. This can be attributed to the effects of an adsorbed water layer separating the solid and air-filled pore system, as discussed in the previous section. This dataset was not fitted using Eq. (1).

Figure 3 shows the SANS data for mature WPC pastes after drying to 54% and 0% RH and after subsequent resaturation. The effects of drying and resaturation (as determined by comparison with the undried mature control) are similar in nature to those shown in Fig. 2 for the young paste, but are smaller in magnitude. This indicates that the hydration products of cement paste undergo less local rearrangement on drying at later hydration ages, in agreement with the observation that bulk irreversible drying shrinkage of cement paste decreases with age.<sup>29</sup>

Greater insight into the microstructural changes caused by drying is obtained by examining the structural parameters associated with the fits using Eq. (1). The value of the primary gel particle diameter from this particular set of fits did not exhibit a statistically significant variation with either age or drying treatment, and had an overall average value of  $a_s = 4.29 \pm 0.09$  nm. The lack of any coarsening of these nanoparticles with time or on drying indicates that they have a surprising degree of physicochemical stability. The solid volume fraction occupied by volume fractal solid material was greater in the mature paste (average  $\phi_{CSH} = 0.206 \pm 0.010$ ) than in the young paste ( $\phi_{CSH} = 0.151 \pm 0.006$ ), but did not exhibit any significant variation with drying treatment. These results support previous findings that the basic nanometer-level structure of C-S-H gel is established at early hydration times<sup>3,25,30</sup> and suggest that this structure is not fundamentally altered by drying. The smooth surface area  $S_0$ , which is more closely related to the particle size of the unhydrated cement powder than to the hydration product morphology, was also statistically unchanged by hydration time or drying (average  $S_0 = 0.77 \pm 0.22$  m<sup>2</sup>/cm<sup>3</sup>).

The remaining model fit parameters for the resaturated pastes are plotted in Fig. 4 as a function of the RH level to which they were initially dried. The uncertainty values shown in Fig. 4 are the standard deviations for the fit parameters obtained for multiple specimens made from the same batch of cement powder and cured under similar conditions. These uncertainties, which account for sample-to-sample microstructural variation and other sources of experimental error, are in most cases significantly larger than the computed uncertainties associated with a particular fit. From Fig. 4 it can be seen that drying decreases  $\xi_v$  and drying to low RH levels decreases  $D_v$  slightly. Drying increases both  $\xi_s$  and  $D_s$  at intermediate RH levels, but has only a very minor effect at low-RH levels. These trends are consistent with a compaction of the volume fractal structure on drying that densifies the layers of hydration product around the original cement grains, leaving the surface fractal component of the microstructure more prominent.

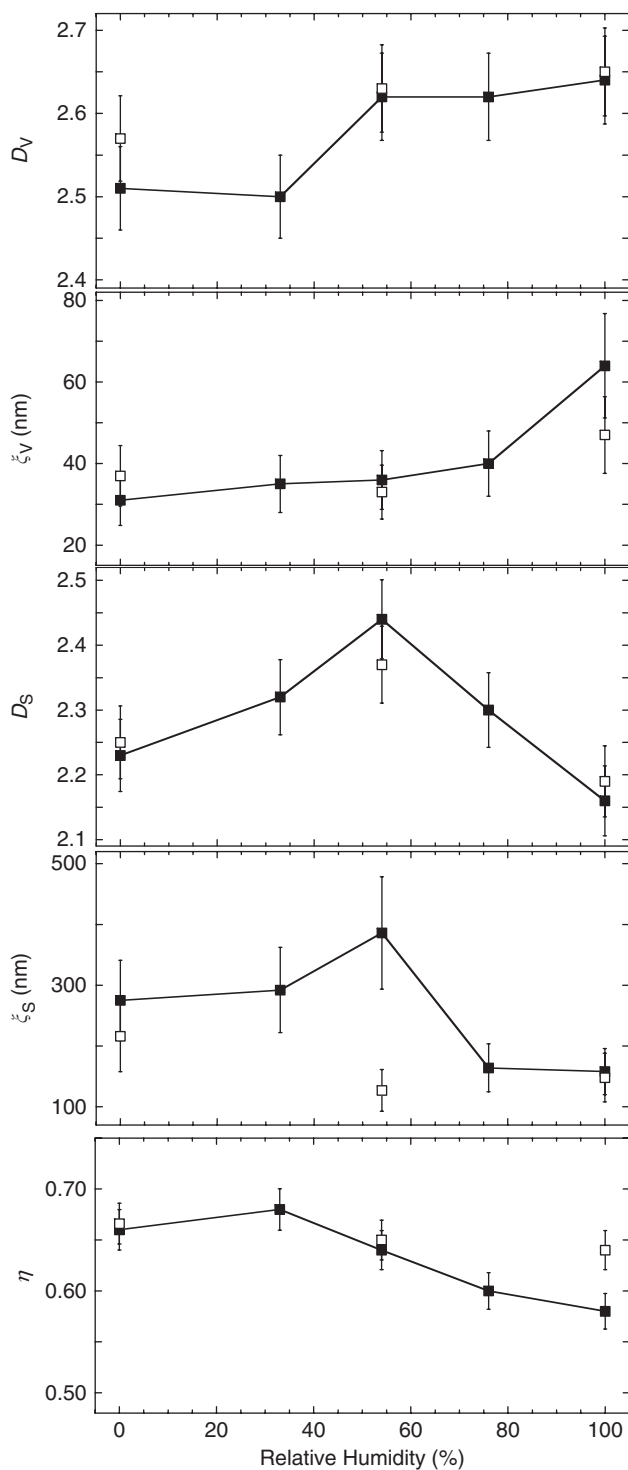


**Fig. 4.** Volume fractal exponent ( $D_v$ ), correlation length ( $\xi_v$ ), surface fractal exponent ( $D_s$ ), correlation length ( $\xi_s$ ) and local packing fraction ( $\eta$ ), determined from fits using Eq. (1), after drying to various relative humidity levels and then resaturating. Solid symbols are for young paste and open symbols are for mature paste. The lines connect the data for the young paste.

The average packing density of solid particles within a single isolated volume fractal region is given by

$$\eta_{VF} = \eta \left( \frac{\xi_V}{R_C} \right)^{D_V-3} \quad (3)$$

where  $R_C$  is close in value to  $a_S$  for nearly spherical particles. In relation to our model, the nanostructure of cement paste is assumed to consist of multiple volume fractal regions of C–S–H gel that grow into each other and overlap during hydration.<sup>2,3</sup> In this case the actual average packing density will be considerably higher than that predicted by Eq. (3). With this in mind, the ratio,  $\eta_{VF}/\eta$ , provides a relative measure of the C–S–H density that is useful for comparative purposes. As shown in Fig. 5,  $\eta_{VF}/\eta$  increases on drying to higher RH levels and resaturating, but no increase is observed following drying to lower RH levels.

The trends shown in Figs. 2–4 can be interpreted to give a more complete picture of the permanent structural changes associated with drying and resaturation of cement paste than has previously been available. Upon drying to higher humidity levels (i.e., 76% and 54% RH) the air/liquid interface surrounds the volume fractal regions of the gel. The capillary pressure difference across the interface,  $\Delta P$ , is given by

$$\Delta P = - \frac{d_f RT}{M_f} \ln RH_f \quad (4)$$

where  $d_f$  and  $M_f$  are the mass density and molecular weight of the pore fluid, respectively, and  $RH_f$  is the RH of the empty pores with respect to the vapor pressure of the pore fluid. Because the pore fluid in cement paste is a rather strong solution of alkalis salts,  $RH_f$  will be somewhat higher than the RH to which the specimen is equilibrated. However, as an upper bound estimate, the values of 76% and 54% RH used in Eq. (4) give capillary pressures of 37 and 83 MPa, respectively. These large pressures compact the gel, increasing its density via a permanent rearrangement of the gel particles that is not reversed when the system is rewetted. This phenomenon is known in the gel literature as “constant rate period” drying,<sup>31</sup> because the decrease in the volume of the gel is equal to the volume of liquid lost by evaporation. A similar result was obtained from a SAXS study of silicate sonogels,<sup>23</sup> which had a lower initial packing density

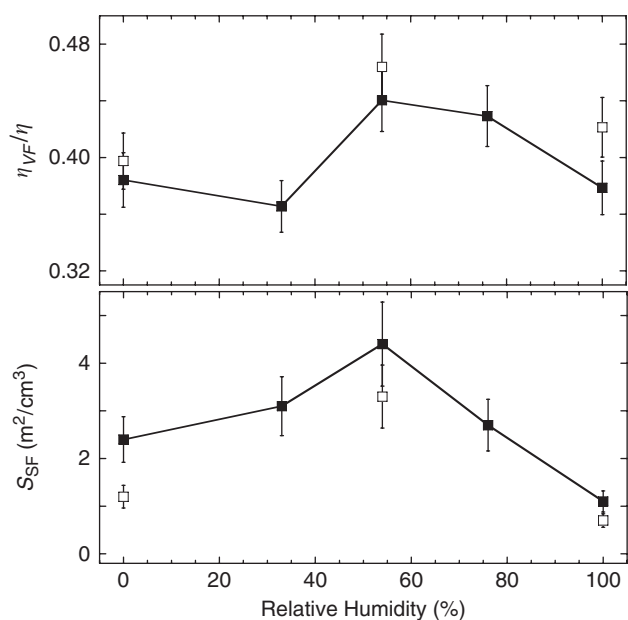


**Fig. 5.** Relative volume fractal packing density (Eq. (3)) and surface fractal surface area (Eq. (5)) after drying to various relative humidity levels and then resaturating. Solid symbols are for young paste and open symbols are for mature paste. The lines connect the data for the young paste.

and thus exhibited relatively larger increases in density on drying.

At the macroscopic level, the bulk shrinkage of cement paste on drying is quite small compared with that of the gel component, generally <1% by volume,<sup>29</sup> due to the restraining effect of nonshrinking solid phases. An increase in the density of the C–S–H gel component should, therefore, be accompanied by an increase in the volume of capillary pores, defined as the larger pores between the regions of volume fractal product. The restrained shrinkage process would thus be expected to open up the capillary pore space and make any surface-fractal component decorating the cement clinker grains more clearly separated from the volume-fractal product. This effect can be observed broadly as an increase in the intensity of the SANS data in the surface fractal-scattering regime at low scattering vectors (Fig. 2). A parameter that can quantify this effect is the fractally rough surface area,  $S_{SF}$ , of the hydration product that decorates or is located on the geometrically smooth surface area,  $S_0$ . This is given by<sup>4</sup>:

$$S_{SF} = S_0 \left( \frac{\xi_S}{R_C} \right)^{D_S-2} \quad (5)$$

where  $R_C$  is again close in value to  $a_S$ . The change in  $S_{SF}$  with drying and resaturation, also shown in Fig. 5, follows a trend similar to that of the packing ratio,  $\eta_{VF}/\eta$ .

The microstructural effects inferred here from the fractal model fits are in good agreement with recent equilibrium drying measurements,<sup>32</sup> where the weight loss of cement paste specimens was measured as they were dried in stepwise fashion using the same procedure as for the SANS specimens discussed here. Comparison of the weight loss results for the first drying cycle and for the second drying cycle (following resaturation) showed that initial drying reduced the volume of pores that empty between 85% and 54% RH (interpreted as the larger gel pores) while increasing the volume of pores emptied above 85% RH (interpreted as the capillary pores).

When the RH inside a gel falls below about 40% RH, air–water menisci become unstable, relieving the capillary stress on the gel, and the remaining liquid water exists primarily as an adsorbed layer around the individual gel particles. The presence of such a layer has a strong effect on the observed scattering response, as can be seen from the very different shape of the SANS data for the specimen dried to 33% RH (see Fig. 2, left). Figure 5 indicates that the volume fractal density for the pastes dried to 33% and 0% RH and then resaturated is not increased. Because drying to 0% and 33% RH requires passing briefly through the higher humidity levels where capillary stresses operate, the lack of a measurable increase in gel density in these specimens indicates that the C–S–H gel does not respond immediately to capillary stresses. This is supported by the fact that the cement paste specimens, despite their small thickness of about 0.5 mm, required several days to equilibrate to the higher RH levels. This may be partly due to the kinetics of moisture transport out of the paste, but likely also reflects the viscoelastic deformation of C–S–H under capillary stress.

The total internal surface area per unit specimen volume,  $S_T$ , obtained independently of the model fits from the scattering at the highest  $q$  (see Eq. (2)), is plotted in Fig. 6. As can be seen from the 100% RH (undried) values, the extended hydration time between 8 days and 3 years caused only a modest increase in surface area, indicating that  $S_T$  is primarily associated with the C–S–H gel that grows into the capillary pore space early in the hydration process. Drying reduced the surface area, with the maximum reduction occurring at 33% RH. Qualitatively similar results for drying of cement paste have been obtained from small-angle X-ray-scattering measurements,<sup>28,33,34</sup> using a different method to calculate the surface area. On resaturating from the higher RH levels the surface area is largely recovered, but at lower RH levels there is a permanent surface area loss. After drying to 0% RH and resaturating, the surface areas of

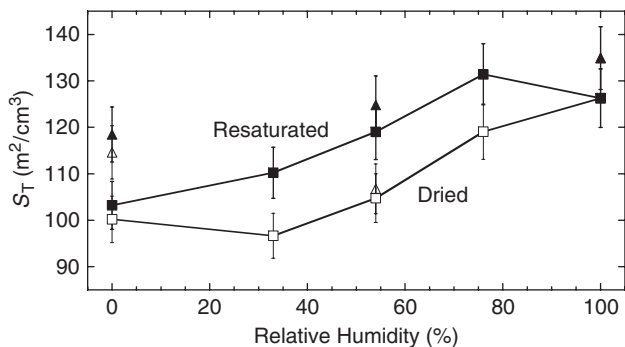


**Fig. 6.** Total internal surface area measured using small-angle neutron scattering after drying (open symbols) and after subsequent resaturation (closed symbols). Squares are for the young paste and triangles are for the mature paste. The lines connect the data for the young paste.

the young and mature pastes decreased by 18% and 12%, respectively.

$S_T$  can be interpreted as a measure of the total amount of scattering interface between the gel particles and the pore fluid accessible to neutrons. Where the gel particles are in contact (or are separated by a thin layer of adsorbed water), there is an effective loss of surface area. Because the gel particle size,  $a_s$ , and total volume fraction,  $\phi_{CSH}$ , obtained from the fractal model fits are not affected by drying, the decrease in  $S_T$  after drying can be attributed to a greater amount of surface lost at particle contacts. The maximum surface area of the volume fractal structure (ignoring particle contacts) inferred from the model fits is given by  $(6/a_s)\phi_{CSH}$ . Using the average values of  $a_s$  and  $\phi_{CSH}$  for the young and mature pastes quoted above results in values of 211 and 287 m<sup>2</sup>/cm<sup>3</sup>, respectively, roughly twice the measured  $S_T$  values. This is a reasonable result for a tightly packed system of particles.

The results shown in Fig. 6 suggest that as the drying RH is lowered, the adjacent gel particles are brought into increasingly close contact, an interpretation that is also supported by the increase in the local packing fraction,  $\eta$ , on drying (see Fig. 4). At higher humidity levels the interparticle spacing could decrease due to a decrease in the disjoining pressure provided by bulk liquid water,<sup>35</sup> a mechanism that can operate in parallel with capillary stresses. At 0% RH removal of the adsorbed layer of water separating the individual gel particles would bring them into direct contact. In the latter case, the  $S_T$  results suggest that the particles do not re-separate on resaturation. A possible explanation for this is that new interlayer space is created when adjacent particles are brought together by drying.<sup>16</sup> The boundary between the adjoining particles is effectively absorbed into the internal structure and, as a result, does not reappear on resaturation.

A consistent trend observed in Figs. 2–6 is that the structural effects of drying are less significant in the mature paste than in the young paste. This is not unexpected, as it is well established that the C–S–H gel phase undergoes chemical aging over time that renders it less susceptible to permanent deformation.<sup>6,36</sup> The present results indicate that the main structural changes that occur on drying, specifically increases in the overall gel density and in the local packing fraction of primary gel particles, also are associated with extended hydration between 8 days and 3 years. Thus, as the packing density of the C–S–H increases over time, the microstructural changes caused by drying are less dramatic.

#### IV. Conclusions

The internal structure of cement paste at a scale of about 1–100 nm can be described as a relatively dense volume fractal gel that is bounded internally by a coarser system of capillary pores. The present study shows that while aging and drying do not alter the essential nanostructural features of cement paste, they do

compact the gel structure making it less susceptible to further irreversible deformation. Application of a practical fractal model to SANS data from dried and resaturated cement paste at two ages allowed the relevant material parameters to be extracted. The observed structural changes on drying could then be related to specific physical mechanisms. For 8-day-old and 2.5-year-old cement pastes reported here, the primary gel particle size is  $4.29 \pm 0.09$  nm and the volume fractal exponent is close to 2.6. On drying to 54% RH and above, the volume fractal structure remains saturated and capillary stresses compact the gel, eliminating the larger interparticle spaces (gel pores) and increasing the average gel density, in agreement with the classical drying theory of gels. This process also increases the surface area of the rough surface fractal interface between the gel and the capillary pore system, an effect that can be attributed to the presence in cement paste of nonshrinking solid phases that restrain the bulk shrinkage.

On drying to 33% RH and below, capillary stresses disappear and the air–water interface penetrates the gel. At 33% RH the presence of a layer of adsorbed water around the individual gel particles has a strong effect on the shape of the SANS data that is eliminated by resaturation. Drying also decreased the total internal surface area (by a maximum of 18% after drying to 0% RH and resaturating), an effect that is interpreted as an increased loss of surface area at particle contacts on drying as adjacent particles are drawn closer together. This can be attributed to a loss of the disjoining pressure of water at higher RH levels, and to the removal of adsorbed water between the particles at lower RH levels.

All of the measured structural changes on drying were more significant in the younger cement paste specimens, indicating that age increases the ability of the C–S–H gel phase to resist structural rearrangement. Whereas some previous work has related aging effects to the increase in silicate polymerization over time, the present results suggest that physical compaction of the C–S–H gel, resulting either from extended hydration within a fixed volume or from capillary stresses on drying, can explain many of the changes associated with aging such as increased resistance to irreversible deformation.

#### References

- G. W. Scherer, "Structure and Properties of Gels," *Cem. Concr. Res.*, **29**, 1149–57 (1999).
- A. J. Allen, R. C. Oberthur, D. Pearson, P. Schofield, and C. R. Wilding, "Development of the Fine Porosity and Gel Structure of Hydrating Cement Systems," *Phil. Mag. B*, **56**, 263–8 (1987).
- A. J. Allen, "Time-Resolved Phenomena in Cements, Clays and Porous Rocks," *J. Appl. Crystallogr.*, **24**, 624–34 (1991).
- A. J. Allen and R. A. Livingston, "Relationship between Differences in Silica Fume Additives and Fine-Scale Microstructural Evolution in Cement Based Materials," *Advn. Cem. Based Mater.*, **8**, 118–31 (1998).
- H. M. Jennings, "A Model for the Microstructure of Calcium Silicate Hydrate in Cement Paste," *Cem. Concr. Res.*, **30**, 101–16 (2000).
- J. J. Thomas and H. M. Jennings, "A Colloidal Interpretation of Chemical Aging of the C–S–H Gel and Its Effects on the Properties of Cement Paste," *Cem. Concr. Res.*, **36**, 30–8 (2006).
- D. P. Bentz, D. A. Quenard, V. Baroghel-Bouny, E. J. Garboczi, and H. M. Jennings, "Modeling Drying Shrinkage of Cement Paste and Mortar Part I: Structural Models from Nanometres to Millimetres," *Mater. Struct.*, **28**, 450–8 (1995).
- P. Acker, "Micromechanical Analysis of Creep and Shrinkage Mechanisms," p. 15 in *Creep, Shrinkage, and Durability Mechanics of Concrete and Other Quasi-Brittle Materials*, Edited by F.-J. Ulm, Z. P. Bazant, and F. H. Wittmann. Elsevier Science Ltd., New York, 2001.
- H. M. Jennings, "Colloid Model of C–S–H and Implications to the Problem of Creep and Shrinkage," *Mater. Struct./Concr. Sci. Eng.*, **37**, 59–70 (2004).
- H. Roper, "Dimensional Change and Water Sorption Studies of Cement Paste"; pp. 74–83 in *Proceedings of the Symposium on Structure of Portland Cement Paste and Concrete*, Highway Research Board Special Report 90, Washington, DC, 1966.
- C. M. Neubauer and H. M. Jennings, "The Use of Digital Images to Determine Deformation Throughout a Microstructure, Part 2: Application to Cement Paste," *J. Mater. Sci.*, **35**, 5751–65 (2000).
- Information on commercial products is given for completeness and does not constitute or imply their endorsement by the National Institute of Standards and Technology.
- C. J. Glinka, J. G. Barker, B. Hammouda, S. Kreuger, J. J. Moyer, and W. J. Orts, "The 30 m Small-Angle Neutron Scattering Instruments at the National Institute of Standards and Technology," *J. Appl. Crystallogr.*, **31**, 430–45 (1998).

- <sup>14</sup>A. Nonat, "The Structure and Stoichiometry of C–S–H," *Cem. Concr. Res.*, **34**, 1521–8 (2004).
- <sup>15</sup>I. G. Richardson, "Tobermorite/Jennite- and Tobermorite/Calcium Hydroxide-Based Models for the Structure of C–S–H: Applicability to Hardened Pastes of Tricalcium Silicate, Dicalcium Silicate, Portland Cement, and Blends of Portland Cement with Blast-Furnace Slag, Metakaolin, or Silica Fume," *Cem. Concr. Res.*, **34**, 1733–77 (2004).
- <sup>16</sup>H. M. Jennings, "Refinements to Colloid Model of C–S–H in Cement: CM-II," *Cem. Concr. Res.*, **38**, 275–89 (2008).
- <sup>17</sup>J. J. Thomas, J. J. Chen, A. J. Allen, and H. M. Jennings, "Effects of Decalcification on the Microstructure and Surface Area of Cement and Tricalcium Silicate Pastes," *Cem. Concr. Res.*, **34**, 2297–307 (2004).
- <sup>18</sup>L. C. Roes and C. G. Schull, "X-Ray Scattering at Small Angles by Finely-Divided Solids. II. Exact Theory for Random Distributions of Spheroidal Particles," *J. Appl. Phys.*, **18**, 308–13 (1947).
- <sup>19</sup>T. Freltoft, J. K. Kjems, and S. K. Sinha, "Power-Law Correlations and Finite-Size Effects in Silica Particle Aggregates Studied by Small-Angle Neutron Scattering," *Phys. Rev. B*, **33**, 269–75 (1986).
- <sup>20</sup>R. Vacher, T. Woignier, and J. Pelous, "Structure and Self-Similarity of Silica Aerogels," *Phys. Rev. B*, **37**, 6500–3 (1988).
- <sup>21</sup>F. Gaboriaud, A. Nonat, D. Chaumont, and A. Craievich, "Aggregation and Gel Formation in Basic Silico-Calco-Alkaline Solutions Studied: A SAXS, SANS, and ELS Study," *J. Phys. Chem. B*, **103**, 5775–81 (1999).
- <sup>22</sup>D. R. Vollet, D. A. Donatti, A. Ibanez Ruiz, and W. C. de Castro, "Structural Study of Aged Saturated Gels Obtained from Tetramethoxysilane Sonohydrolysis with Different Water/Tetramethoxysilane Molar Ratio," *Phys. Rev. B*, **67**, 184207 (2003).
- <sup>23</sup>D. R. Vollet, D. A. Donatti, A. Ibanez Ruiz, and H. Maceti, "Small-Angle X-Ray Scattering Study of the Structural Evolution of the Drying of Sonogels with the Liquid Phase Exchanged by Acetone," *Phys. Rev. B*, **69**, 094203 (2004).
- <sup>24</sup>H. D. Bale and P. W. Schmidt, "Small-Angle X-Ray Scattering Investigation of Submicroscopic Porosity with Fractal Properties," *Phys. Rev. Lett.*, **53**, 596–9 (1984).
- <sup>25</sup>J. J. Thomas, H. M. Jennings, and A. J. Allen, "The Surface Area of Cement Paste as Measured by Neutron Scattering—Evidence for Two C–S–H Morphologies," *Cem. Concr. Res.*, **28**, 897–905 (1998).
- <sup>26</sup>A. J. Allen, J. J. Thomas, and H. M. Jennings, "Composition and Density of Nanoscale Calcium–Silicate–Hydrate in Cement," *Nat. Mater.*, **6**, 311–6 (2007).
- <sup>27</sup>J. C. Li, D. K. Ross, L. D. Howe, K. L. Stefanopoulos, J. P. A. Fairclough, R. Heenan, and K. Ibel, "Small-Angle Neutron-Scattering Studies of the Fractal-Like Network Formed During Desorption and Adsorption of Water in Porous Materials," *Phys. Rev. B*, **49**, 5911–7 (1994).
- <sup>28</sup>R. E. Beddoe and K. Lang, "Effect of Moisture on Fractal Dimension and Specific Surface of Hardened Cement Paste by Small-Angle X-Ray Scattering," *Cem. Concr. Res.*, **24**, 605–12 (1994).
- <sup>29</sup>S. Mindess, J. F. Young, and D. Darwin, *Concrete*, 3rd edition, Prentice Hall, Upper Saddle River, NJ, 2003.
- <sup>30</sup>D. R. Vollet and A. F. Craievich, "Effects of Temperature and of the Addition of Accelerating and Retarding Agents on the Kinetics of Hydration of Tricalcium Silicate," *J. Phys. Chem. B*, **104**, 12143–8 (2000).
- <sup>31</sup>C. J. Brinker and G. W. Scherer, *Sol–Gel Science*. Academic Press, New York, 1990.
- <sup>32</sup>H. M. Jennings, J. J. Thomas, J. S. Gvrenov, G. Constantinides, and F.-J. Ulm, "A Multi-Technique Investigation of the Nanoporosity of Cement Paste," *Cem. Concr. Res.*, **37**, 329–36 (2007).
- <sup>33</sup>J. J. Volkl, R. E. Beddoe, and M. J. Setzer, "The Specific Surface of Hardened Cement Paste by Small-Angle X-Ray Scattering—Effect of Moisture Content and Chlorides," *Cem. Concr. Res.*, **17**, 81–7 (1987).
- <sup>34</sup>J. J. Thomas, H. M. Jennings, and A. J. Allen, "The Surface Area of Hardened Cement Paste as Measured by Various Techniques," *Concr. Sci. Eng.*, **1**, 45–64 (1999).
- <sup>35</sup>F. Beltzung and F. H. Wittmann, "Role of Disjoining Pressure in Cement Based Materials," *Cem. Concr. Res.*, **35**, 2364–70 (2005).
- <sup>36</sup>Z. P. Bazant, A. B. Huggaard, S. Baweja, and F. J. Ulm, "Microprestress Solidification Theory for Concrete Creep. I: Aging and Drying Effects," *J. Eng. Mech., ASCE*, **123**, 1188–94 (1997). □